npj | space exploration

Article

https://doi.org/10.1038/s44453-025-00009-6

Complex impact processes on the Moon's farside recorded by Chang'e-6 low-Ti basalt

Check for updates

Jing Yang[1], Wei Du[2,3] ✉, Dongyang Ju[2,4], Rui Li[1], Jianzhong Liu[1,3], Shirong Liu[5], Yuanyun Wen[1], Yang Li[1,3], Xiongyao Li[1,3] & Yun Liu[2,3,6] ✉

Thousands of craters on the lunar surface offer a unique perspective to investigate the impact process of the inner Solar System. However, the mid-late-stage impact history of the Moon since ~3.1 Ga remains poorly constrained due to the sample scarcity from this period exhibiting significant shock effects. Here, we present diverse shock metamorphism features in basalt clasts returned by the Chang'e-6 mission from a low-Ti mare unit on the lunar farside that formed approximately 2.8 billion years ago. High-pressure phases seifertite, stishovite, coesite, and maskelynite, as well as quartz cluster in a shock melt pocket and compositional oscillations in pyroxenes within these samples, reveal at least four distinct pressure−temperature−time paths, indicating complex impact processes on the lunar farside. The high peak pressures (~30−40 GPa) recorded in these samples are comparable with lunar meteorites, suggesting no significant difference in impact intensity between the Moon's two hemispheres since its mid-evolutionary stage.

According to lunar crater chronology models, the impact flux on the Moon was high during its early history and declined rapidly between ~3.9–3.1 Ga and then probably remained at a low and nearly constant rate[1,2]. Nevertheless, collisions of asteroids or comets with the Moon have continued to occur since ~3.1 Ga in its mid-late stage, resulting in the formation of massive craters on the lunar surface such as Copernicus, Tycho, and Aristarchus, while also transporting impact ejecta over long distances[1,3–6]. However, a considerable amount of available lunar samples formed during this period are mare basalts returned from the nearside of the Moon. These basalts show little information about impact processes, especially those with high-pressure minerals are very rare[5,7,8]. Natural high-pressure minerals are formed under extreme pressure conditions, typically found in terrestrial and extraterrestrial materials that underwent impact events (such as rocks on the lunar surface and heavily shocked meteorites)[5,9] or deep in the interior of larger planetary bodies (like the Earth) associated with deeper metamorphism[10]. The formation processes of high-pressure minerals in shocked materials are closely related to the pressure–temperature–time (P−T−t) paths of impact events. Therefore, high-pressure minerals and their formation mechanisms are extensively utilized for estimating shock conditions[11]. The limitations of the sampling area and the lack of research on the shock metamorphism of lunar basalt samples including high-pressure mineral phases have restricted our in-depth understanding of the impact history of the Moon during its mid-late evolution.

The South Pole–Aitken (SPA) basin, a home to millions of craters, serves as an ideal region for investigating the shock effects generated on planetary bodies. This study presents various shock metamorphism features in basalt clasts collected by the Chang'e-6 (CE-6) mission from a low-Ti basalt unit formed at ~2.8 billion years ago[12–14] within the SPA basin[15]. We elucidate the nature, occurrence, and formation mechanisms of shock melt pockets, high-pressure phases, and shock-induced chemical compositional oscillation of pyroxene grains. These identified shock metamorphism features provide insightful and critical information for constraining the complex impact P−T−t history of the lunar material, as well as the impact processes and exogenic geological evolution of the mid-late stage of the Moon.

Results

Three representative basalt clasts (B1, B2, and B3) from the scooped soil sample CE6C0300YJFM001 show various shock metamorphism features (Fig. 1). Basalt clasts in CE-6 returned samples predominantly consist of

[1]Center for Lunar and Planetary Sciences, Institute of Geochemistry, Chinese Academy of Sciences, Guiyang, China. [2]State Key Laboratory for Critical Mineral Research and Exploration, Institute of Geochemistry, Chinese Academy of Sciences, Guiyang, China. [3]Center for Excellence in Comparative Planetology, Chinese Academy of Sciences, Hefei, China. [4]College of Earth and Planetary Sciences, University of Chinese Academy of Sciences, Beijing, China. [5]State Key Laboratory of Environmental Geochemistry, Institute of Geochemistry, Chinese Academy of Sciences, Guiyang, China. [6]Research Center for Planetary Science, College of Earth Sciences, Chengdu University of Technology, Chengdu, China. ✉e-mail: duwei@mail.gyig.ac.cn; liuyun@vip.gyig.ac.cn

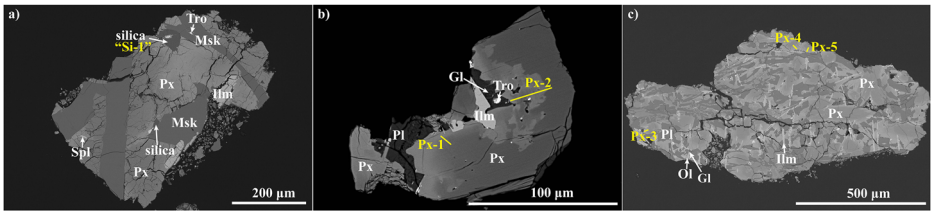

Fig. 1 | Back-scattered electron (BSE) images of CE-6 low-Ti basalt clasts with shock features in CE6C0300YJFM001. a Clast B1 exhibits a poikilitic texture. **b** Clast B2, two yellow lines represent positions of EPMA profile analyses. **c** Clast B3 exhibits a poikilitic to porphyaceous texture; three yellow lines represent positions of EPMA profile analyses. Px pyroxene, Msk maskelynite, Ilm ilmenite, Spl spinel, Tro troilite, Pl plagioclase, Gl Si-K-rich glass, and Ol olivine.

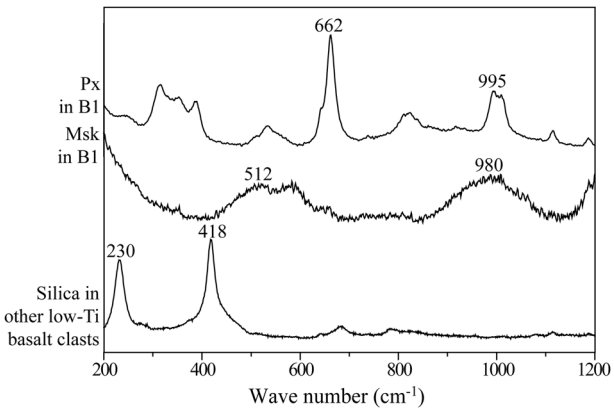

Fig. 2 | Representative Raman spectra with background correction of silicates in the CE-6 low-Ti basalt clasts. Px pyroxene, Msk maskelynite.

local low-Ti basalt with minor amounts of exotic very low-Ti basalt and high-Al basalt[12–14,16,17]. The consistency in chemical characteristics of constituent minerals (pyroxene and plagioclase) in these three studied basalt clasts with CE-6 low-Ti basalt[12,16,17] strongly supports a local origin (Supplementary Fig. 1 and Supplementary Fig. 2).

Shock melt pocket and high-pressure mineral phases

The low-Ti basalt clast B1 is mainly composed of pyroxene, plagioclase, and ilmenite, as well as minor amounts of silica, spinel, Fe-sulfide, and Si-K-rich glass (Fig. 1a). The clast shows a poikilitic texture and contains high-pressure polymorphs and a shock melt pocket with an area of ~20×10 μm. Plagioclase grains generally show a smooth appearance, and most of them have been transformed into maskelynite, while pyroxenes are highly fractured but show no phase transition (Fig. 2 and Supplementary Fig. 3).

The shock melt pocket in clast B1 is embedded in a pyroxene grain and adjacent to a silica grain "Si-1" (Fig. 3a and Supplementary Fig. 4). From center to rim, the major constituents of this shock melt pocket are relict silica fragments, needle-shaped stishovite and assemblages of nano-size stishovite embedded in Fe-Ca-rich glasses, and fine-grained pyroxene polymorphs (Fig. 3a, b and Supplementary Fig. 5). The margin of pyroxene adjacent to the melt pocket shows lattice distortion (Fig. 3c). Silica crystal cluster is observed to grow along the crack cutting through the shock melt pocket and is best indexed with the *P3_221* quartz crystal structure (Fig. 3d and Supplementary Fig. 4).

Grain "Si-1" shows tweed-like texture and contains multiple sets of crystallographically oriented amorphous lamellae, including a sub-orthogonal pattern consisting of two sets of lamellae and a sub-hexagonal pattern consisting of three sets of lamellae (Fig. 4a). As the distance from the shock melt pocket increases, this silica grain generally transformed from angular α-cristobalite crystallites (up to 1 mm) (Supplementary Fig. 4b and Supplementary Fig. 6a) to nano-size (10−50 nm) granular phases that exhibit triple junction with coesite inside (Fig. 4c and Supplementary Fig. 6d), and to high-pressure crystalline phases set within the framework of amorphous lamellae (Fig. 4b). The crystallites within the sub-orthogonal framework of amorphous lamellae are seifertite in spindle or short prismatic shape with dimensions of ~30−200 nm and those within the sub-hexagonal framework are stishovite exhibiting triangular morphology with size up to ~100 nm (Fig. 4d and Supplementary Fig. 6b, c).

Oscillatory zoning of pyroxene in low-Ti basalt clasts

Pyroxenes in CE-6 low-Ti basalt exhibit chemical variation from Mg-rich cores to Fe-rich rims (Supplementary Fig. 1a) similar to those in Apollo 12 ilmenite basalts, in which case the Wo values of pyroxene display slight oscillation[18]. However, some pyroxene grains in CE-6 low-Ti basalt clasts do not follow this simple crystallization trend. For example, one pyroxene grain in clast B3, hereinafter is referred to as "Px-3" (Fig. 1c and Supplementary Fig. 7b) shows similar Mg-Fe variation but dramatic change in its Wo value (Fig. 5a). Its core is augite ($En_{32.5}Fs_{31.5}Wo_{36.0}$) and subsequently mantled by pigeonite ($En_{33.2}Fs_{50.6}Wo_{16.2}$), but the rim is Fe-rich augite with higher Wo value ($En_{4.9–25.7}Fs_{49.2–70.9}Wo_{25.2–33.2}$, Supplementary Table 1). Another pyroxene grain in clast B2, hereinafter referred to as "Px-2" (Fig. 1b and Supplementary Fig. 7a), exhibits oscillatory zoning of Mg# [molar Mg/(Mg + Fe) × 100]. From the interior to the rim, its Mg# decreases from 57.4 to 15.6, then increases to 33, followed by a decrease to ~5 to its rim that is adjacent to the mesostasis pocket (mainly consists of Si-K-rich glass and troilite) and the Wo value changes systematically with the Mg# (Fig. 5b).

Discussion

Although high-pressure minerals have been reported in lunar meteorite samples[19–26] and Apollo and Chang'e-5 returned lunar regolith[5,7,8], the high-pressure polymorphs of silica present in this study are the first to be reported in mare basalt samples returned from the Moon. Stishovite crystallites in the shock melt pocket exhibit acicular morphology and random orientation, suggesting the genesis of crystallization from SiO_2-rich melt during shock compression when the pressure remained high[27,28]. The peak temperature should be higher than 1900−3000 K to form the basaltic shock melt[29,30]. The single appearance of stishovite without seifertite or coesite indicates that the peak pressure was at least 10 GPa but lower than ~45 GPa[31,32]. On the other hand, the tweed-like texture of the grain "Si-1" indicates that the three high-pressure silica polymorphs coesite, stishovite, and seifertite should have formed through a solid-state transformation mechanism[5,22,33], as we expect by impact shock generated in large impacts. The relatively large (~1 mm) angular crystallites are all α-cristobalite, indicating that grain "Si-1" is primarily α-cristobalite, the same as those in CE-6 low-Ti basalt clasts (Fig. 2 and Supplementary Fig. 3). Seifertite crystallites coherently grow with α-cristobalite as shown by their parallelly orientated grain boundaries[31,34,35] (Fig. 4b). Stishovites are bounded by three sets of amorphous lamellae, not compatible with the tetragonal twinning texture of α-cristobalite, but their overall extension directions are parallel to those of seifertite (Fig. 4d). According to the relationship between the orientation of mineral lattices, we speculate that α-cristobalite in clast B1 changed to seifertite during the compression stage of an impact event, then a proportion of the seifertite (~30%) was heated by the high temperature condition (~1100 K) generated by the impact and transformed to stishovite. Considering the formation mechanism of seifertite and stishovite and the heat sensitivity of these two phases, the peak pressure experienced by the grain "Si-1" could be ~11−40 GPa[5,36,37]. In short, the different high-pressure polymorphs of silica

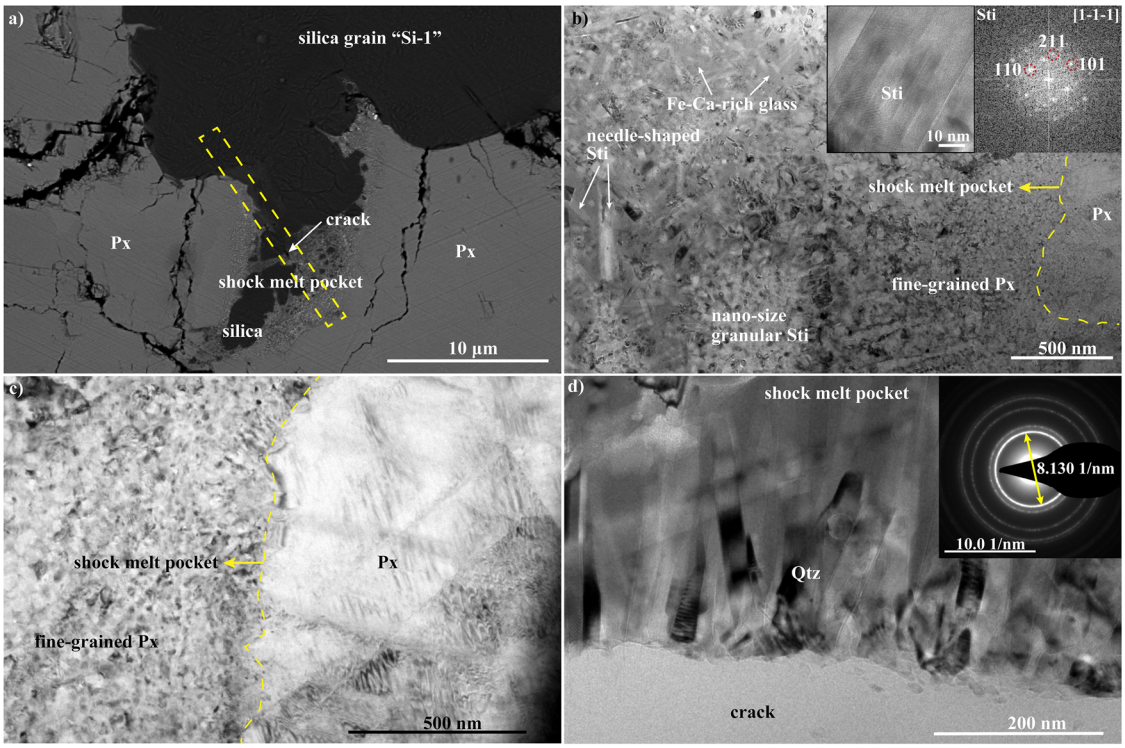

Fig. 3 | BSE and Transmission electron microscopy (TEM) images of the shock melt pocket in basalt clast B1. a The occurrence of the shock melt pocket; the yellow rectangle shows the location of the FIB section. The BSE and TEM images of the whole FIB section are shown in Supplementary Fig. 4. **b** The bright-field (BF)-TEM image, high-resolution TEM image, and Fast Fourier Transform (FFT) pattern of needle-shaped stishovite crystallites embedded in Fe-Ca-rich glasses within the shock melt pocket. **c** The margin of the pyroxene grain adjacent to the shock melt pocket shows lattice distortion. **d** Quartz cluster crystallized along the crack cutting through the shock melt pocket. Yellow dashed lines in **b** and **c** represent boundaries of the shock melt pocket. Px pyroxene, Sti stishovite, Qtz quartz.

in clast B1 record different P−T−t paths. Considering the temperature nonuniformity caused by the shock event, one major impact with peak pressure ~11−40 GPa is capable of causing the formation of the above-mentioned different polymorphs of silica. This impact event could be the same shock that has been experienced by the whole rock as indicated by the widespread maskelynite (~25−30 GPa; refs. 38,39) outside the shock melt pocket.

Another polymorph of silica, a quartz cluster along the crack cutting through the shock melt pocket (Fig. 3d and Supplementary Fig. 4) should have formed from a post-impact thermal event, thus a second impact event for the following reasons. If the quartz cluster crystallized from the shock melt and penetrated the crack after the pressure released during the same impact event, quartz grains should not only be restricted to growth close to the crack but also distribute in other regions such as the edge of the shock melt pocket, which is inconsistent with the observations (Fig. 3b and Supplementary Fig. 5). In addition, shock melt pockets and veins are generally formed through localized melting of rocks caused by the extreme heat and pressure of an impact event, then the injecting of melts into cracks or fractures which quickly cools and solidifies[40]. Thus, crack cutting through the shock melt pocket in clast B1 likely results from a subsequent impact or other mechanisms to compress and break the CE-6 low-Ti basalt rock after the impact event that generated high-pressure silica polymorphs. And the quartz cluster growing along the crack also likely formed in a subsequent thermal event after the high-pressure polymorphs-generating impact event. On the other hand, although post-shock annealing with high temperatures and slow cooling rates could lead to the back-transformation of high-pressure phases[41–44], it is difficult for quartz to form from stishovite in the small (only ~10 μm in width) shock melt pocket because of rapid cooling rates[42]. Moreover, the inconsistent orientation between quartz (oriented) and stishovite (random) does not support thermal metamorphism to trigger back-transformation of stishovite to quartz either. In contrast, a subsequent impact event could not only be responsible for the formation of a crack as mentioned above, but also can generate a larger temperature increase at the phase interfaces relative to surroundings[45,46]. The heterogeneous shock-induced heating can explain the remelting of the shock melt pocket restricted along the crack, followed by crystallization of sub-micron-sized quartz from this SiO_2-rich melt. In short, the different polymorphs of silica in clast B1 record at least two impact events after the crystallization of the CE-6 low-Ti basalt.

Although high-pressure polymorphs are often used as diagnostic indicators of shock conditions[11], they are rare in returned lunar samples. Previous studies indicate that shock features such as mosaic extinction and mechanical twinning observed in pyroxene subjected to impact are also valuable for constraining the shock conditions[37,46]. As a major component of lunar rocks, pyroxene can constitute up to 63% modal abundance in mare basalts[47,48], highlighting the importance of investigating the shock metamorphism characteristics of pyroxene in returned lunar samples.

Almost all pyroxene grains in CE-6 low-Ti basalt clasts are chemically zoned following the cooling and fractionation trend (Fig. 5) as those present in mare basalts[49]. One excepted pyroxene grain "Px-2" shows special Mg-Fe oscillatory zoning (Fig. 5b) that is nearly absent in the lunar magmatic environment[50]. Several mechanisms can generate compositional oscillations in minerals within basalts: (1) elements with slow diffusion rate during a relatively fast cooling such as phosphorus and REEs exhibit oscillatory zoning within zircon crystals[51]; (2) vigorous convection and magma replenishment happened prior to the basaltic magma eruption as proposed by Elardo & Shearer (2014) to explain the Mg# oscillatory zoning in pyroxene phenocrysts from mare basaltic meteorite Northwest Africa 032[52]; (3) changes in the magma composition as phases come in and out of the crystallization sequence; and (4) shock-induced partial melting followed by recrystallization. It is challenging to cause the Mg# oscillatory zoning in pyroxene during crystallization in a closed parent magma system, as the

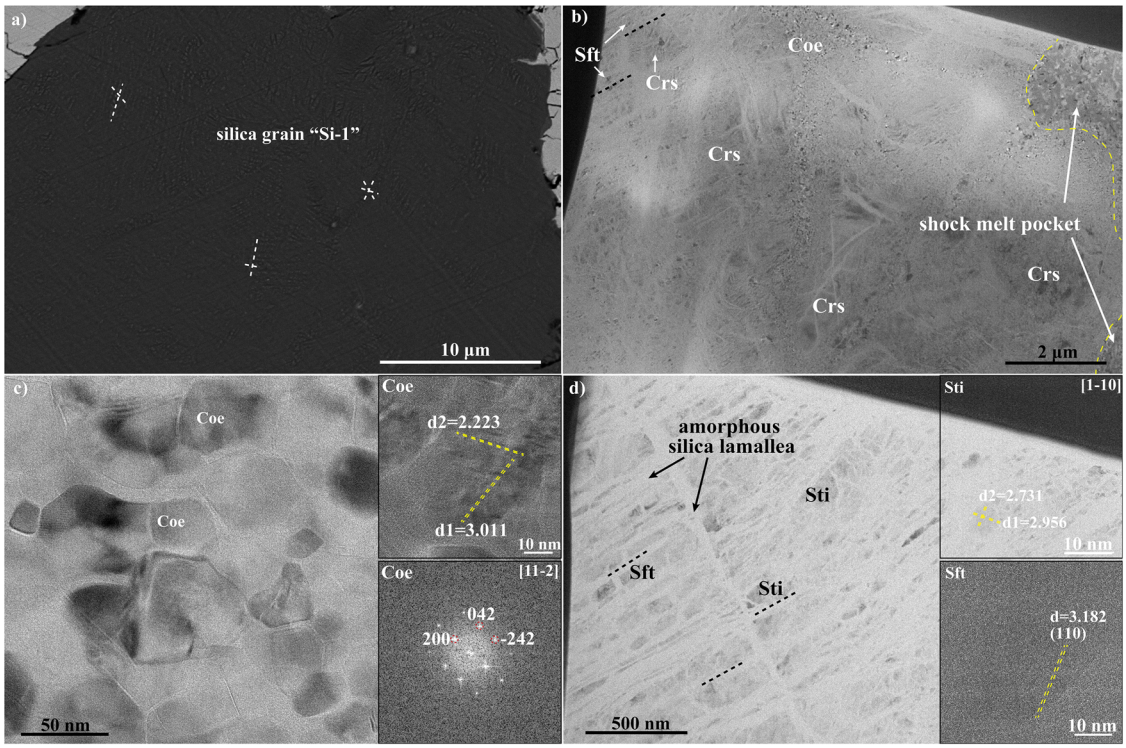

Fig. 4 | BSE and TEM images of seifertite-stishovite-coesite-bearing silica grain "Si-1" in basalt clast B1. a The white dashed lines represent the orientations of the amorphous silica lamellae. **b** Alpha-cristobalite with angular morphology, and the black dashed line denotes the orientation of the α-cristobalite boundary. **c** Coesite crystallites exhibit a triple junction with interplanar spacing (d-spacing) marked by yellow dashed lines. **d** Seifertite and stishovite with amorphous silica lamella cutting through, whose orientation is marked by the black dashed lines. Yellow dashed lines represent d-spacing. Crs α-cristobalite, Coe coesite, Sft seifertite, and Sti stishovite.

Fe–Mg interdiffusion rates in clinopyroxene at igneous temperatures are relatively fast[53]. In addition, oscillatory zoning in minerals formed by mechanisms (1) and (2) is generally concentric, and boundaries between adjacent zoning are regular[51,52,54], which is inconsistent with the Mg-Fe oscillatory zoning in grain "Px-2" (Supplementary Fig. 7b). Ilmenite is an important rock-forming mineral in mare basalts and generally crystallizes later than pyroxene[55,56]. However, its crystallization resulting in a decrease of FeO content in silicate melt and Mg# oscillation in pyroxene has not been discovered in mare basalts. Moreover, mechanisms (1)−(3) involve crystallization of parent magma, which is generally a relatively long and equilibrated process. Thus, these three mechanisms encounter difficulty in explaining why only the "Px-2" grain has Mg-Fe oscillation and other pyroxenes in the same clast do not. In contrast, the heterogeneous temperature distribution during impact[45] could explain the distinct melt behavior of pyroxene grains within several hundred microns (Fig. 5b).

Another special pyroxene grain "Px-3" exhibits obvious Ca oscillation from core to rim with normal Mg and Fe chemical trend (Fig. 5a). Calcium oscillation in pyroxene could be preserved mainly as the result of relatively fast cooling because of the relatively slow diffusion rate of Ca^{2+} in clinopyroxene[57,58]. If this is the case, the more prominent change of CaO content in "Px-3" compared to other pyroxene grains in clast B3 indicates that it has experienced a much more rapid cooling process, resulting in non-equilibrium on CaO content. It is difficult to have significant cooling rate differences within the submillimeter to millimeter scale during magma crystallization. And as discussed above, mechanisms (2) and (3) will have a similar influence on the CaO profile of all pyroxene grains in the clast B3, not just on that of pyroxene "Px-3". Instead, like grain "Px-2", impact could cause a localized "hot spot" that partially melted "Px-3" grain, followed by recrystallization while other pyroxenes in the same basalt clast remain in a solid state without partial melting.

The absence of maskelynite and high-pressure polymorphs of pyroxene in clasts B2 and B3 (Supplementary Fig. 3) suggests that the peak shock pressure experienced by their host rocks is lower than 15 GPa[39], while the peak temperature of local areas within these two clasts could have reached ~2050−2400 K to melt clinopyroxene[59]. These impact processes are different from the ones mentioned above that cause the formation of high-pressure silica polymorphs and oriented quartz cluster, revealing the great potential of compositional oscillations in pyroxene grains for constraining the P–T–t paths experienced by silicate rocks, which received insufficient attention previously.

The diverse shock metamorphism features in CE-6 low-Ti basalt clasts record multiple impact processes on the low-Ti basalt unit inside the Apollo basin within SPA. Using shock wave physics models[60] (Supplementary Text 1 and Supplementary Text 2), we estimate the diameter of the impactor, the impact velocities, and the size of the craters formed during these impact events (Supplementary Table 2, details are described in supplementary materials). The impactor and target are set to be ordinary chondrites (the crater size is not sensitive to impactor materials; ref. 61) and basalts, respectively. An impactor with diameter of ~0.7−0.8 km hitting basalt with velocity of ~3−3.4 km/s can generate shock pressure of 25−30 GPa (the peak pressure of clast B1) with shock duration of ~0.22−0.27 s and form the largest crater (diameter: ~1.7 km) on the low-Ti mare unit where the CE-6 mission landed[62]. Furthermore, the shock duration is constrained to be no shorter than 0.1 s according to the time−temperature−transformation (TTT) curve of seifertite and stishovite[36] and the time-sensitive kinetics for the formation of seifertite. In this case, the impactor cannot be smaller than ~0.3 km to generate a shock pressure of 25−30 GPa, and the diameter of the resulting crater could be at least ~0.8 km. For impact peak pressure ≤15 GPa to form the chemical oscillation in pyroxenes, the estimated impactor size is not larger than ~0.95 km, and the impactor velocity could not exceed ~2.1 km/s, indicating a distinct impact event from the formation of high-pressure polymorphs of silica in clast B1. Combined with the formation of quartz cluster in clast B1 triggered by another impact event and great difference

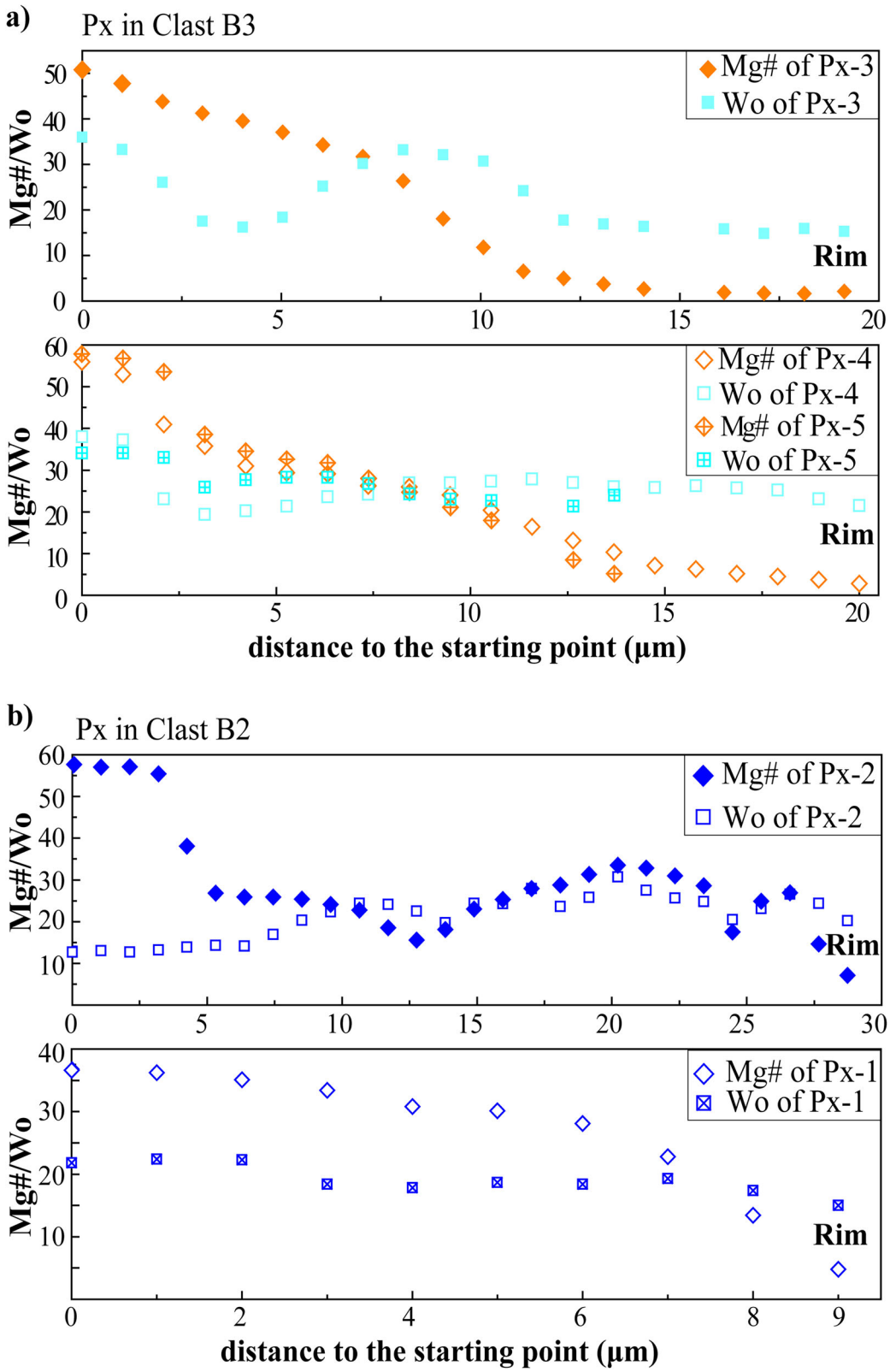

Fig. 5 | Major element compositions of pyroxenes in CE-6 low-Ti basalt clasts. a The variation of Mg# and Wo value from grain interior to the rim in pyroxenes (Px) within basalt clast B3. **b** The variation of Mg# and Wo value from interior to the rim in pyroxenes within basalt clast B2.

in cooling rate of partially melted pyroxenes within clasts B2 and B3 (~300 K/day at ~2000 K for cooling of "Px-2" vs. ~0.5–1.0 K/day at ~2000 K for cooling of "Px-3", Supplementary Text 3 and Supplementary Text 4; Supplementary Fig. 8), shock metamorphism features in the three CE-6 low-Ti basalt clasts reveal at least four impacts by hundred-meters-sized asteroids on the lunar farside within an area of ~5.8×10^3 km^2 (ref. 63) since the crystallization of low-Ti mare basalt in SPA basin at ~2.8 Ga ago.

The existence of high-pressure silica polymorphs in CE-6 low-Ti basalt indicates that impacts producing craters of a relatively modest 1.7 km in size

can generate peak shock pressure ~25−30 GPa. If this is the case, high-pressure minerals could be common in lunar rocks, which is inconsistent with the actual situation in lunar basalts returned by Apollo missions. For this scientific issue, we thought that the discovery of high-pressure polymorphs in lunar samples may be more relevant to the preservation conditions. High-pressure polymorphs are easily disturbed and transform back to their related low-pressure phases during subsequent massive impact events that occur on the Moon's surface. The low-Ti mare unit where the CE-6 mission landed is younger (~2.8 Ga[12–14]) than the Apollo basalt samples (>3.3 Ga). Furthermore, impact craters on CE-6 low-Ti mare unit are smaller (≤1.7 km) and fewer (only 18 craters with diameter ~0.8−1.7 km) than those on Apollo-landed mare units. This may be conducive to the preservation of high-pressure polymorphs in CE-6 low-Ti basalt.

Apollo samples commonly show a lower shock degree than lunar meteorites (5−30 GPa vs. >28 GPa), and previous studies proposed that it is due to either sampling bias or location bias[64–66]. Nevertheless, returned samples by Chang'e missions from the lunar nearside[5] and from the SPA basin on the lunar farside (this study) contain high-pressure mineral phases and have undergone peak shock pressure (up to ~30−40 GPa) comparable with lunar meteorites from random locations on the lunar surface. Thus, there might be no significant shock degree difference generated on the two hemispheres of the Moon. Moreover, the diverse shock metamorphism features in CE-6 low-Ti basalt demonstrate that lunar surface minerals exposed to relatively large impacts are altered by shock, and fractured and compressed to an extent in which these processes probably changed the physical and elemental properties of the rock-forming minerals. Several recent studies have also revealed that impact events have significant effects on the mechanical properties of minerals in lunar and HED meteorites[67,68]. It is necessary to research further the macro- and microstructural mechanical properties of extraterrestrial rocks, which will serve as a foundational resource for future space exploration, as well as mining techniques and science.

Methods

Sample preparation

The CE-6 scooped soil sample CE6C0300 (YJFM001, 100 mg), allocated by the China National Space Administration, was used in this study. Regolith fragments were hand-picked under a binocular microscope and mounted in BUEHLER EpoxiCure™ 2 epoxy resin to make several mounts, then polished for petrological and mineralogical studies.

Analytical methods

The polished mounts were carbon-coated and observed using an FEI Scios dual-beam focused ion beam/scanning electron microscope (FIB-SEM) equipped with an energy dispersive spectrometer (EDS) at the Center for Lunar and Planetary Sciences (CLPS), Institute of Geochemistry, Chinese Academy of Sciences (IGCAS) in Guiyang. Raman spectra of mineral phases in basalt clasts were collected using a Renishaw InVia-532 laser Raman spectroscopy at CLPS, IGCAS. The laser beam, with a wavelength of 785 nm, was focused to ~1 μm on the sample surface. Each spectrum comprised a scan from 200 to 1200 cm^{-1} with a total counting time of 100 s, excited with a laser power of 4.4 mW. The Raman spectra that were used to confirm mineral phases in this study are raw data (Supplementary Table 3) processed by baseline correction using LabSpec software.

The major element compositions of mineral phases (pyroxene, plagioclase, ilmenite, olivine, silica, and Si-K-rich glass) in each CE-6 basalt clast were analyzed using an electron probe micro-analyzer (EPMA; JEOL JXA8530F-plus) at the State Key Laboratory for Critical Mineral Research and Exploration, IGCAS. The conditions of EPMA are as follows: accelerating voltage of 15 kV, probe current of 10 nA, focused beam and peak counting time of 20 s, except Na and K were counted for 10 s, and Ba was counted for 30 s. Natural and synthetic minerals and glasses were used as standards. Detection limits for oxides were 0.01–0.03 wt%. Data were calibrated using the ZAF method.

The FIB-SEM of FEI Scios at CLPS, IGCAS was used to cut a FIB slice for the transmission electron microscopy (TEM) observations. An accelerating voltage of 30 kV and beam currents of 15 nA–500 pA were applied during the thinning process. Bright-field images and selected area electron diffraction (SAED) patterns were acquired by an FEI Titan Tecnai G2 F20 transmission electron microscopy (TEM) at the State Key Laboratory of Environmental Geochemistry, IGCAS, operated at 200 kV. In addition, an FEI Talos F200XS/TEM operating at 200 kV combined with a SuperX EDS system at Suzhou Institute of Nano-Tech and Nano-Bionics, CAS, was used for bright and dark field images, high-resolution TEM (HRTEM) images, and quantitative mapping. The EDS elemental mapping and quantitative analysis were performed by using the Esprit software from the Bruker corporation. All the investigations in TEM were conducted at low electron dose to mitigate the sample damage.

Data availability

All data in this study are included in this published article and supplementary information file. For the data policy, all of the data above for this paper are also available in Figshare (https://doi.org/10.6084/m9.figshare.29064986).

Received: 20 May 2025; Accepted: 24 July 2025;
Published online: 24 October 2025

References

1. Warren, P. H. & Taylor, G. J. in *Treatise on Geochemistry (Second Edition)* 213–250 (Elsevier, 2014).
2. Neukum, G., Ivanov, B. A. & Hartmann, W. K. Cratering records in the inner Solar System in relation to the lunar reference system. *Space Sci. Rev.* **1**, 55–86 (2001).
3. Hiesinger, H. et al. How old are young lunar craters? *J. Geophys. Res. Planets* **117**, 2011JE003935 (2012).
4. Iqbal, W., Hiesinger, H. & van der Bogert, C. H. Geological mapping and chronology of lunar landing sites: Apollo 12. *Icarus* **352**, 113991 (2020).
5. Pang, R. et al. New occurrence of seifertite and stishovite in Chang'E-5 regolith. *Geophys. Res. Lett.* **49**, e2022GL098722 (2022).
6. Yang, J. et al. Significance of silicate liquid immiscibility for the origin of young highly evolved lithic clasts in Chang'E-5 regolith. *Geochim. Cosmochim. Acta* **340**, 189–205 (2023).
7. Kaneko, S. et al. Discovery of stishovite in Apollo 15299 sample. *Am. Mineral.* **100**, 1308–1311 (2015).
8. Qiu, M. et al. Discovery of a highly shocked alkali suite clast in the Changae-5 lunar soils. *Icarus* **429**, 116448 (2024).
9. Tomioka, N. & Miyahara, M. High-pressure minerals in shocked meteorites. *Meteorit. Planet. Sci.* **52**, 2017–2039 (2017).
10. Bykova, E. et al. Metastable silica high pressure polymorphs as structural proxies of deep Earth silicate melts. *Nat. Commun.* **9**, 4789 (2018).
11. Gillet, P. & El Goresy, A. Shock Events in the Solar System: the message from minerals in terrestrial planets and asteroids. *Annu. Rev. Earth Planet. Sci.* **41**, 257–285 (2013).
12. Cui, Z. et al. A sample of the Moon's far side retrieved by Chang'e-6 contains 2.83-billion-year-old basalt. *Science* **386**, 1395–1399 (2024).
13. Zhang, Q. W. L. et al. Lunar farside volcanism 2.8 billion years ago from Changae-6 basalts. *Nature* **643**, 356–360 (2024).
14. Che, X. et al. Isotopic and compositional constraints on the source of basalt collected from the lunar farside. *Science* **387**, 1306–1310 (2025).
15. Li, C. et al. Nature of the lunar farside samples returned by the Chang'E-6 mission. *Natl. Sci. Rev.* **11**, nwae328 (2024).

16. Yin, C. et al. Petrogenesis of Chang'e-6 basalts and implication for the young volcanism on the lunar farside. *Astrophys. J. Lett.* **981**, L2 (2025).
17. Shen, D. et al. Petrogenesis of Chang'E-6 basalts and implication for multi-episode volcanism in the lunar farside basin. *Earth Planet. Sci. Lett.* **659**, 119335 (2025).
18. Papike, J. J., Hodges, F. N., Bence, A. E., Cameron, M. & Rhodes, J. M. Mare basalts: crystal chemistry, mineralogy, and petrology. *Rev. Geophys.* **14**, 475–540 (1976).
19. Barrat, J. A. et al. Lithium behavior during cooling of a dry basalt: an ion-microprobe study of the lunar meteorite Northwest Africa 479 (NWA 479). *Geochim. Cosmochim. Acta* **69**, 5597–5609 (2005).
20. Zhang, A.-C. et al. Petrogenesis of lunar meteorite Northwest Africa 2977: constraints from in situ microprobe results. *Meteorit. Planet. Sci.* **45**, 1929–1947 (2010).
21. Ohtani, E. et al. Coesite and stishovite in a shocked lunar meteorite, Asuka-881757, and impact events in lunar surface. *Proc. Natl. Acad. Sci. USA* **108**, 463–466 (2011).
22. Miyahara, M. et al. Discovery of seifertite in a shocked lunar meteorite. *Nat. Commun.* **4**, 1737 (2013).
23. Chen, J. et al. Petrogenesis and shock metamorphism of basaltic lunar meteorites Northwest Africa 4734 and 10597. *J. Geophys. Res. Planets* **124**, 2583–2598 (2019).
24. Fritz, J. et al. Donwilhelmsite, [$CaAl_4Si_2O_{11}$], a new lunar high-pressure Ca-Al-silicate with relevance for subducted terrestrial sediments. *Am. Mineral.* **105**, 1704–1711 (2020).
25. Xing, W. et al. Discovery of reidite in the lunar meteorite Sayh al Uhaymir 169. *Geophys. Res. Lett.* **47**, e2020GL089583 (2020).
26. Zhang, A.-C. et al. Widespread tissintite in strongly shock-lithified lunar regolith Breccias. *Geophys. Res. Lett.* **48**, e2020GL091554 (2021).
27. Langenhorst, F. & Poirier, J.-P. Anatomy of black veins in Zagami: clues to the formation of high-pressure phases. *Earth Planet. Sci. Lett.* **184**, 37–55 (2000).
28. Spray, J. G. & Boonsue, S. Quartz–coesite–stishovite relations in shocked metaquartzites from the Vredefort impact structure, South Africa. *Meteorit. Planet. Sci.* **53**, 93–109 (2018).
29. Hirose, K., Fei, Y., Ma, Y. & Mao, H.-K. The fate of subducted basaltic crust in the Earth's lower mantle. *Nature* **397**, 53–56 (1999).
30. Hu, J. & Sharp, T. G. Formation, preservation and extinction of high-pressure minerals in meteorites: temperature effects in shock metamorphism and shock classification. *Prog. Earth. Planet. Sci.* **9**, 6 (2022).
31. Dubrovinsky, L. S. et al. Pressure-induced transformations of cristobalite. *Chem. Phys. Lett.* **333**, 264–270 (2001).
32. Langenhorst, F. & Deutsch, A. Shock metamorphism of minerals. *Elements* **8**, 31–36 (2012).
33. El Goresy, A., Dubrovinsky, L., Sharp, T. G. & Chen, M. Stishovite and post-stishovite polymorphs of silica in the shergotty meteorite: their nature, petrographic settings versus theoretical predictions and relevance to Earth's mantle. *J. Phys. Chem. Solids.* **65**, 1597–1608 (2004).
34. Dera, P., Lazarz, J. D., Prakapenka, V. B., Barkley, M. & Downs, R. T. New insights into the high-pressure polymorphism of SiO2 cristobalite. *Phys. Chem. Miner.* **38**, 517–529 (2011).
35. Černok, A. et al. Compressional pathways of α-cristobalite, structure of cristobalite X-I, and towards the understanding of seifertite formation. *Nat. Commun.* **8**, 15647 (2017).
36. Kubo, T., Kato, T., Higo, Y. & Funakoshi, K.-i Curious kinetic behavior in silica polymorphs solves seifertite puzzle in shocked meteorite. *Sci. Adv.* **1**, e1500075 (2015).
37. Stöffler, D., Hamann, C. & Metzler, K. Shock metamorphism of planetary silicate rocks and sediments: proposal for an updated classification system. *Meteorit. Planet. Sci.* **53**, 5–49 (2018).
38. Fritz, J. et al. Shock pressure calibration for lunar plagioclase. *42nd Lunar and Planetary Science Conference*, held March 7–11, 2011 at The Woodlands, Texas. LPI contribution, No. 1608, p.1196 (Lunar and Planetary Institute, 2011).
39. Hu, J., Asimow, P. D., Liu, Y. & Ma, C. Shock-recovered maskelynite indicates low-pressure ejection of shergottites from Mars. *Sci. Adv.* **9**, eadf2906 (2023).
40. Walton, E. L. & Herd, C. D. K. Dynamic crystallization of shock melts in Allan Hills 77005: implications for melt pocket formation in Martian meteorites. *Geochim. Cosmochim. Acta* **71**, 5267–5285 (2007).
41. Chen, M., Xie, X., El Goresy, A., Wopenka, B. & Sharp, T. G. Cooling rates in the shock veins of chondrites: constraints on the (Mg, $Fe)_2SiO_4$ polymorph transformations. *Sci. China. Ser. D.* **41**, 522–528 (1998).
42. Hu, J. & Sharp, T. G. Back-transformation of high-pressure minerals in shocked chondrites: low-pressure mineral evidence for strong shock. *Geochim. Cosmochim. Acta* **215**, 277–294 (2017).
43. Miyahara, M., Yamaguchi, A., Ohtani, E., Tomioka, N. & Kodama, Y. Complicated pressure–temperature path recorded in the eucrite Padvarninkai. *Meteorit. Planet. Sci.* **56**, 1443–1458 (2021).
44. Zhang, A.-C. et al. Formation and decomposition of vacancy-rich clinopyroxene in a shocked eucrite: new insights for multiple impact events. *Geochim. Cosmochim. Acta* **329**, 38–50 (2022).
45. Sharp, T. G. & DeCarli, P. S. in *Meteorites and the Early Solar System II*, 653–677 (University of Arizona Press, 2006).
46. Fritz, J., Greshake, A. & Fernandes, V. A. Revising the shock classification of meteorites. *Meteorit. Planet. Sci.* **52**, 1216–1232 (2017).
47. Taylor, G. J. et al. in *Lunar Sourcebook: A User's Guide to the Moon*. 183–284 (Cambridge University Press, 1991).
48. Papike, J. J., Ryder, G. & Shearer, C. K. in *Planetary Materials, Reviews in Mineralogy*, 5-1-5-234 (The Mineralogical Society of America, 1998).
49. Karner, J., Papike, J. J. & Shearer, C. K. Comparative planetary mineralogy: pyroxene major- and minor-element chemistry and partitioning of vanadium between pyroxene and melt in planetary basalts. *Am. Mineral.* **91**, 1574–1582 (2006).
50. Head, J. W. & Wilson, L. Lunar mare volcanism: stratigraphy, eruption conditions, and the evolution of secondary crusts. *Geochim. Cosmochim. Acta* **56**, 2155–2175 (1992).
51. Yang, W. et al. Phosphorus-controlled trace element distribution in zircon revealed by NanoSIMS. *Contrib. Mineral. Petr.* **171**, 28 (2016).
52. Elardo, S. M. & Shearer, C. K. Jr. Magma chamber dynamics recorded by oscillatory zoning in pyroxene and olivine phenocrysts in basaltic lunar meteorite Northwest Africa 032. *Am. Mineral.* **99**, 355–368 (2014).
53. Müller, T., Dohmen, R., Becker, H. W., ter Heege, J. H. & Chakraborty, S. Fe–Mg interdiffusion rates in clinopyroxene: experimental data and implications for Fe–Mg exchange geothermometers. *Contrib. Mineral. Petr.* **166**, 1563–1576 (2013).
54. Shore, M. & Fowler, A. D. Oscillatory zoning in minerals; a common phenomenon. *Can. Mineral* **34**, 1111–1126 (1996).
55. Curran, N. M. et al. The early geological history of the Moon inferred from ancient lunar meteorite Miller Range 13317. *Meteorit. Planet. Sci.* **54**, 1401–1430 (2019).
56. Wang, Y. et al. Petrogenesis of the Northwest Africa 4734 basaltic lunar meteorite. *Geochim. Cosmochim. Acta* **92**, 329–344 (2012).
57. Dimanov, A., Jaoul, O. & Sautter, V. Calcium self-diffusion in natural diopside single crystals. *Geochim. Cosmochim. Acta* **60**, 4095–4106 (1996).
58. Zhang, X., Ganguly, J. & Ito, M. Ca-Mg diffusion in diopside: tracer and chemical inter-diffusion coefficients. *Contrib. Mineral. Petr.* **159**, 175–186 (2010).

59. Gasparik, T. Melting experiments on the enstatite-diopside join at 70–224 kbar, including the melting of diopside. *Contrib. Mineral. Petr.* **124**, 139–153 (1996).
60. Melosh, H. J. *Impact Cratering: A Geologic Process*. (Oxford University Press, 1989).
61. Pang, R.-L., Zhang, A.-C., Wang, S.-Z., Wang, R.-C. & Yurimoto, H. High-pressure minerals in eucrite suggest a small source crater on Vesta. *Sci. Rep.* **6**, 26063 (2016).
62. Yue, Z. et al. Geological context of the Chang'e-6 landing area and implications for sample analysis. *Innovation* **5**, 100663 (2024).
63. Gou, S. et al. Complex basalt evolution in the Chang'e-6 landing area. *Earth Planet. Sci. Lett.* **648**, 119091 (2024).
64. Rubin, A. E. Maskelynite in asteroidal, lunar and planetary basaltic meteorites: an indicator of shock pressure during impact ejection from their parent bodies. *Icarus* **257**, 221–229 (2015).
65. Pernet-Fisher, J. F., Joy, K. H., Martin, D. J. P. & Donaldson Hanna, K. L. Assessing the shock state of the lunar highlands: implications for the petrogenesis and chronology of crustal anorthosites. *Sci. Rep.* **7**, 5888 (2017).
66. Joy, K. H. et al. Lunar meteorites. *Rev. Mineral. Geochem.* **89**, 509–562 (2023).
67. Peña-Asensio, E., Trigo-Rodríguez, J. M., Sort, J., Ibáñez-Insa, J. & Rimola, A. Mechanical properties of minerals in lunar and HED meteorites from nanoindentation testing: Implications for space mining. *Meteorit. Planet. Sci.* **59**, 1297–1313 (2024).
68. Grèbol-Tomàs, P. et al. Mechanical softening of lunar olivine probed via nanoindentation and high-pressure X-ray diffraction measurements. *Geosci. Front.* **16**, 102110 (2025).

Acknowledgements

We appreciate all the staff of the Chang'e-6 mission, and their great effort makes this work possible. We thank China National Space Administration (CNSA) for providing the CE-6 sample CE6C0300YJFM001. We thank Bing Mo and Xiang Li for their assistance with Raman and EPMA analyses. Dr. M.-T. Niu is thanked for the TEM observations and quantitative mapping analyses. Funding: Jing Yang discloses support for the research of this work from the National Natural Science Foundation of China [grant number 42373041] and [grant number 42441822]. Wei Du discloses support for the research of this work from the National Natural Science Foundation of China [grant number 41973058] and [grant number 42473052]. Yun Liu discloses support for the research of this work from the National Key Research and Development Program of China [grant number 2024YFF0807500]. Yang Li discloses support for the research of this work from the National Natural Science Foundation of China [grant number 42441804] and the Foundation of the President of the Chinese Academy of Sciences [grant number QYJ-2025-0103]. Jianzhong Liu discloses support for the research of this work from the Major Scientific and Technological Special Project of Guizhou Province [Grant number QKH-ZDZX(2024)-016]. Xiongyao Li discloses support for the research of this work from Guizhou Provincial 2019 Science and Technology Subsidies [grant number GZ2019SIG].

Author contributions

J.Y., W.D., and Y. Liu designed this research; J.Y. characterized the petrography and mineral chemistry of basalt samples in CE-6 regolith samples; J.Y. performed the EDS and EPMA analyses and the Raman experiment. J.Y. and D.-Y.J. carried out the modeling of cooling rate calculation; Y.-Y.W. performed the making of FIB section; J.Y., R.L., and S.-R.L. performed the TEM observations; Y. Li applied the CE-6 samples and gave the suggestions for the TEM observations and SAED pattern analyses; J.-Z.L. provided the crater size and distribution information on the low-Ti mare unit where the CE-6 mission landed; X.-Y.L. suggested the formation mechanisms of high-pressure phases in CE-6 low-Ti basalt; J.Y. and W.D. wrote the manuscript. All authors contributed to the preparation of the manuscript. All authors have read and approved the manuscript.

Competing interests

The authors declare no competing interests. W.D. is on the editorial board of *npj Space Exploration* but was not involved in the peer review process or decision making for the paper.

Additional information

Supplementary information The online version contains supplementary material available at https://doi.org/10.1038/s44453-025-00009-6.

Correspondence and requests for materials should be addressed to Wei Du or Yun Liu.